RSC Advances

PAPER

View Article Online
View Journal | View Issue

Cite this: *RSC Adv.*, 2021, **11**, 21851

A GGA + U investigation into the effects of cations on the electromagnetic properties of transition metal spinels†

Chunyu Li,[a] Peng Li,[a] Leyun Li,[a] Dingjia Wang,[a] Xingfa Gao *[b] and Xuejiao J. Gao *[a]

Received 9th May 2021
Accepted 7th June 2021

DOI: 10.1039/d1ra03621a

rsc.li/rsc-advances

Spinel oxides are promising low-cost catalysts with manifold and controllable physicochemical properties. Trial and error strategies cannot achieve the effective screening of high-performance spinel catalysts. Therefore, unraveling the structure–performance relationship is the foundation for their rational design. Herein, the effects of cations in tetrahedral and octahedral sites on the electronic structures of spinels were systematically investigated using GGA + U calculations based on ACr_2O_4 (A = Mn, Fe, Co, Ni, and Zn) and Zn/LiB_2O_4 (B = Cr, Mn, Fe, Co and Ni). The results indicate that the octahedrally coordinated B cations have notable influence on the electronic structures of spinels. The Jahn–Teller active ions Fe^{2+}, Ni^{2+}, Mn^{3+}, Ni^{3+}, Cr^{4+} and Fe^{4+} can remarkably reduce the band gaps of spinels and even change their electroconductibilities. These results will provide theoretical insights into the electronic properties of 3d transition metal spinels.

Introduction

Spinels were initially regarded as precious stones such as the famous Black Prince's Ruby and Timur Ruby. In 1915, the first report of the crystal structure of a spinel lifted the veil of gems.[1] The spinel structure is formulated AB_2X_4, where A and B are tetrahedrally and octahedrally coordinated metal cations, respectively, and X is an anion (typically O or F). Fig. 1A presents the structural model of normal AB_2O_4, where O^{2-} has a close-packed array and A^{2+} and B^{3+} ions are in tetrahedral and octahedral cages formed by the oxygens, respectively. Each unit cell contains eight formula units and has a composition of $A_8B_{16}O_{32}$.

Spinels contain a large number of species and embody almost all main group metals and transition metals.[2,3] The benefits of spinels, such as tunable composition, electron configurations, valence and magnetic states as well as low cost, make them increasingly attractive in optical, electromagnetic, information technology, environmental science, energy storage and conversion fields.[4–6] Recently, their intrinsic enzyme-mimicking activities, such as peroxidase-, oxidase-, superoxide dismutase- and catalase-like activities, cast light on broad biomedical applications.[7–19]

However, trial and error strategies cannot achieve the effective screening of high-performance spinels, which hinder the rational design spinel catalysts. Recently, Xu *et al.* developed cations in octahedral sites as an effective descriptor to predict spinel catalysts with high oxygen-reduction reaction (ORR) and oxygen-evolution reaction (OER) performance.[20] Although progresses have been achieved,[21–25] efforts are still needed to reveal the unambiguous structure–function relationship. The rational design roots in the physicochemical properties. According to previous reports, the electronic configuration of metal cations,[26] the occupation of tetrahedral and octahedral sites[20] and the spin orders[22,23,27] are key factors affecting the geometric and electronic properties of spinels.

Herein, to investigate the effects of cations in tetrahedral and octahedral sites on the electronic structures of spinels, three series of spinels (Fig. 1B), where the metals on A and B sites have continuously varying electronic conformations, namely ACr_2O_4 (A = Mn, Fe, Co, Ni, and Zn) and Zn/LiB_2O_4 (B = Cr, Mn, Fe, Co and Ni), were investigated as the model system. The B cations in the LiB_2O_4 series have two valence states, particularly half B^{3+} and half B^{4+}. The results indicate that the magnetism of spinels depends on the indirect exchange of cations (J_{MM}). The configuration of octahedrally coordinated B cations has notable influence on the electronic structures of spinels. The results presented here provide insights into the physicochemical properties of spinels.

[a]College of Chemistry and Chemical Engineering, Jiangxi Normal University, Nanchang, 330022, China. E-mail: gaoxj@jxnu.edu.cn

[b]Laboratory of Theoretical and Computational Nanoscience, CAS Key Laboratory for Biomedical Effects of Nanomaterials and Nanosafety, National Center for Nanoscience and Technology, Chinese Academy of Sciences, Beijing, 100190, China . E-mail: gaoxf@nanoctr.cn

† Electronic supplementary information (ESI) available: The Hubbard U_{eff} (eV) values employed for metal ions, the calculated energies for spinels with different magnetic states and the optimized structures for the spinels. See DOI: 10.1039/d1ra03621a

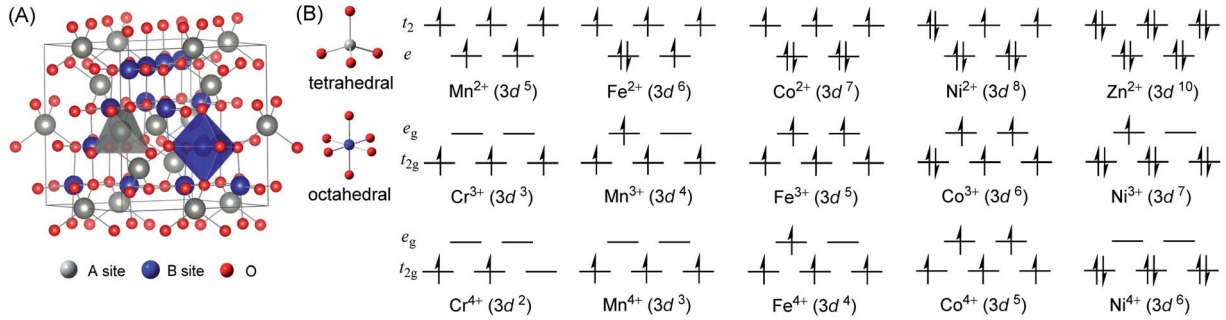

Fig. 1 (A) The geometric structure of AB_2O_4 spinel. The A^{2+} ions (grey spheres) and the B^{3+} ions (light blue spheres) are in tetrahedral and octahedral cages formed by the oxygen atoms (red spheres). (B) Electron configurations of A^{2+} and B^{3+} ions with increasing 3d electron.

Methods

Calculations were performed under periodic boundary conditions employing the Vienna *Ab initio* Simulation Package (VASP).[28] Projector-augmented wave (PAW)[29] pseudopotentials and Perdew–Burke–Ernzerhof (PBE)[30] exchange-correlation functional of generalized gradient approximation (GGA) were used to describe the interactions between core electrons. Both geometric optimizations and density of states (DOS) analysis were performed using a standard Monkhorst–Pack grid[31] sampling at $7 \times 7 \times 7$. An energy cut-off was set to 450 eV and the convergence thresholds for the electronic structure and forces were set to 10^{-5} eV and 0.02 eV $Å^{-1}$, respectively. The Hubbard U correction[32,33] was used to make the strong coulomb interactions of d electrons more accurate. Following a literature survey,[25,34–36] the U_{eff} values used for 3d metals are shown in Table S1.†

Results and discussion

To verify the ground states for spinels, initial magnetic states illustrated in Fig. 2 with different spin orders were set for geometric optimizations. All initial structures with eight formula units in one unit cell are crystallized in the $Fd\bar{3}m$ space group (No. 227). The calculated energies for all magnetic states are listed in Table S1,† and the geometric structures of the ground states are illustrated in Figure S1.† The optimized physicochemical characteristics including the ground state (GS), lattice parameters, band gap (E_g) and magnetic moments on tetrahedral and octahedral metal atoms (MO and MT) are listed in Table 1.

Ferrite spinels are of technological interest because of their magnetic ordering. How the unpaired spins of metal ions are coupled determines the magnetism of spinels. The 2nd column of Table 1 lists the magnetic orders for the ground states of the spinels. The Goodenough–Kanamori rules[37–44] predict the local magnetism, which results from the superexchange coupling of the electron spins of transition metal ions. The O^{2-} ions shared by two metal ions can mediate the coupling of spins by superexchange, as shown in Fig. 3.

In spinel, each magnetic ion at site A has 12 magnetic ions at site B to undergo A–B exchanges and each B site ion has 6 A site ions undergo A–B exchanges. Moreover, the angles between A and B (ϕ_{AB}) are close to 180° and the distances between A and B are the shortest. Therefore, the A–B exchanges (Fig. 3a and b) are the strongest, followed by B–B exchanges (Fig. 3c and d) and A–A (Fig. 3e) exchanges are the weakest. The above rules can profoundly explain the magnetic ground states of spinels listed in Table 1. For ACr_2O_4 (A = Mn, Fe, Co, and Ni), the exchange between A and its nearest B are the strongest leading to opposite spin orders on A and B. If the A–B and B–B exchanges (Fig. 3b–d) are strong enough to oppositely arrange the spin orders of A–B and B–B, the final magnetism of the spinel will be AFM like $MnCr_2O_4$, where the Mn^{2+} has the largest net spins, as shown in Fig. 1b. Spinels ACr_2O_4 (A = Fe, Co, and Ni) have strong A–B but weak B–B exchanges, which finally leads to the FM′ magnetic states. For Zn/LiB_2O_4 (A = Zn and Li; B = Cr, Mn, Fe, Co, and Ni), the B–B exchanges are the dominating interactions because Zn^{2+} and Li^+ have fully and empty occupied 3d orbitals.

The B–B exchanges in Zn/LiB_2O_4 (B = Cr, Mn, Fe, and Co) are stronger than those in $Zn/LiNi_2O_4$, which leads to their AFM and FM states.

The 3–4 columns of Table 1 list the lattice parameters for the spinels calculated in present work and as reported by previous experiments. The relative errors (δ) between them are less than

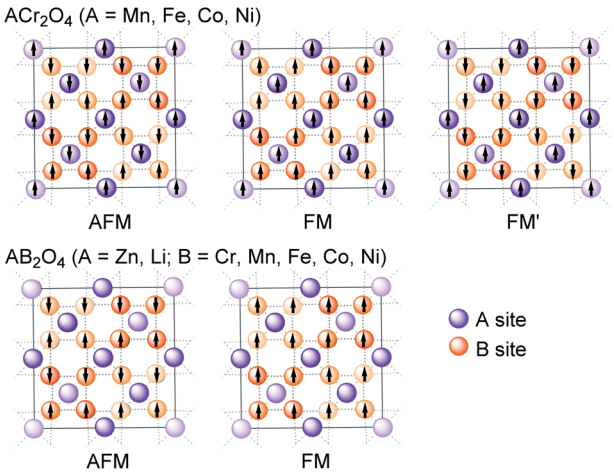

Fig. 2 Magnetic states initially set for optimizations. There are three initial states, namely AFM, FM and FM′, for ACr_2O_4 (A = Mn, Fe, Co, and Ni). The net magnetic moments for A, B and the whole bulk are zero in the AFM state. In the FM state, the magnetic moments of A and B are in the same direction, while in the opposite directions in the FM′ state. There are two magnetic states for Zn/LiB_2O_4 (B = Cr, Mn, Fe, Co, and Ni) since Zn^{2+} and Li^+ have no unpaired 3d electron.

Table 1 Summary of the calculated ground states (GS), lattice parameters, band gaps (E_g, in eV) and the magnetic moments (μ) on the metal atoms in tetrahedral (MT) and octahedral (MO) environments[a]

		Lattice parameters			E_g		Magnetic moment (μ)			
Spinel	GS	Cal.	Exp.	δ (%)	Theor.	Exp.	μ_{MT}	n_{3d_MT}	μ_{MO}	n_{3d_MO}
$MnCr_2O_4$	AFM	8.46	8.44[45]	0.237	2.91	2.50[46]	4.56	3.67	2.95	2.11
$FeCr_2O_4$	FM′[47]	$a = c = 8.41$, $b = 8.39$	8.38[48]	0.239	2.15	1.95[49] 2.90[49]	3.69	2.82	2.95	2.11
$CoCr_2O_4$	FM′[50]	8.36	8.33[50]	0.360	2.87	2.77[51]	2.70	1.88	2.95	2.11
$NiCr_2O_4$	FM′[35]	$a = 8.30$, $b = c = 8.36$	$a = 8.18$, $b = 8.17$, $c = 8.57$[27]	—	2.39	1.70[52]	1.75	1.42	2.96	2.12
$ZnCr_2O_4$	AFM[53]	8.34	8.31[53]	0.361	3.30	1.66[54] 3.61[55]	0.0	0.00	2.95	2.11
$ZnMn_2O_4$	AFM[53]	$a = b = 8.63$, $c = 8.0$	$a = b = 8.10$, $c = 9.24$[53]	—	0.22	1.28[56]	0.00	0.00	3.79	2.92
$ZnFe_2O_4$	AFM[53]	8.39	8.46[57]	0.827	1.60	1.78[58]	0.00	0.00	4.25	3.37
$ZnCo_2O_4$	AFM	$a = c = 8.38$, $b = 8.08$	8.05[53]	—	1.11	1.71[59] 2.77[59]	0.00	0.00	3.25	2.40
$ZnNi_2O_4$	FM	8.17	—	—	—		0.00	0.00	1.39	0.71
$LiCr_2O_4$	AFM	$a = c = 8.16$, $b = 8.24$	8.11[60]	—	1.03		0.00	0.00	2.90/2.03	2.07/1.26
$LiMn_2O_4$	AFM[61]	$a = c = 8.32$, $b = 8.00$	8.25[62,63]	—	0.69	0.58[64]	0.00	0.00	3.77/2.96	2.90/2.12
$LiFe_2O_4$	AFM	$a = b = 8.32$, $c = 8.05$	—	—	—		0.00	0.00	4.20/3.61	3.32/2.75
$LiCo_2O_4$	AFM[26]	$a = 8.06$, $b = c = 8.19$	7.99,[26] 8.153[65]	—	0.24		0.00	0.00	3.45/2.78	2.59/1.95
$LiNi_2O_4$	FM	$a = 8.06$, $b = c = 7.80$	8.04[66]	—	0.44		0.00	0.00	1.05/0.01	0.45/0.00

[a] The number of unpaired 3d electrons (n_{3d}) of the metals are derived from μ ($\mu = \sqrt{n(n+2)}$). The lattice parameters measured by experiments are also listed for comparison.

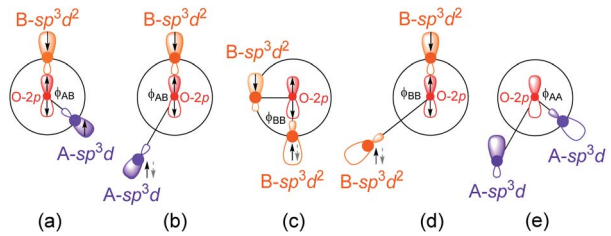

Fig. 3 Five cases of indirect exchange interactions between A–B (a and b), B–B (c and d) and A–A (e).

1.00%. In ACr_2O_4 (A = Fe, Co, and Ni), A = Fe and Ni are Jahn–Teller active ions[23] with orbital degeneracy and slightly collective distortion are observed in the relaxed unit cell. For spinels with nonmagnetic A site ions, namely Zn/LiB_2O_4 (B = Cr, Mn, Fe, and Co), the antiferromagnetic J_{B-B} exchange interactions lead to highly frustrated ground states on the pyrochlore sublattice. This frustration can be released by the spin-Jahn–Teller effect[67,68] and lead to lattice distortions. The calculated magnetic moments (μ) on MO and MT are also listed in Table 1. The number of unpaired 3d electrons (n_{3d}) can be derived from $\mu = \sqrt{n(n+2)}$. Although the calculated n_{3d} are smaller than the theoretical values illustrated in Fig. 1B, it does not affect the reliability of the calculations since the rational tendency is predicted.

To investigate the influences induced by cation A and B on the electronic structures of spinels, we calculated the projected density of states (PDOS) of ACr_2O_4 (A = Mn, Fe, Co, Ni, Zn) and Zn/LiB_2O_4 (B = Cr, Mn, Fe, Co and Ni). The band gaps were also calculated and are listed in Table 1. Fig. 4A presents the PDOS for ACr_2O_4 (A = Mn, Fe, Co, Ni, and Zn), which indicate that cation A has limited impact on the electronic structures of spinels. The E_g of ACr_2O_4 differs in a narrow range from 2.30 to 3.30 eV. $Mn/Co/ZnCr_2O_4$ has Jahn–Teller inactive A ions and thus have similar electronic structures. The Jahn–Teller active Fe^{2+} and Ni^{2+} can reduce E_g because the e^3 configuration of Fe^{2+} raises the valence-band maximum (VBM) and the t_{2g}^4 configuration of Ni^{2+} lowers the conduction band minimum (CBM). The above-mentioned results can be verified by the fact that the partial charge populations, corresponding to the VBM of $FeCr_2O_4$ and the CBM of $NiCr_2O_4$ are mainly contributed by the e orbital of Fe^{2+} and the t_2 orbital of Ni^{2+}.

Fig. 4B and C indicate that the electronic configuration of cation B has notable influence on the electronic structure of spinel. The Jahn–Teller active Mn^{3+}, Ni^{3+}, Cr^{4+} and Fe^{4+} can remarkably reduce the E_g of spinels and even change the semiconductor to metal and half-metal. The notable differences between $ZnCr_2O_4$ and $LiCr_2O_4$ indicate that the Jahn–Teller active Cr^{4+}in $LiCr_2O_4$ lowers the CBM to the Fermi level and notably narrows the band gap of $LiCr_2O_4$. The reason is that CBM in $ZnCr_2O_4$ is contributed by the e_g orbital but by the t_{2g} orbital with a lower energy level in $LiCr_2O_4$. In $ZnMn_2O_4$, VBM and CBM are contributed by the two e_g orbitals, namely d_{z^2} and $d_{x^2-y^2}$, of Mn^{3+}. The introduction of Mn^{4+} in $LiMn_2O_4$ does not change the contributions of e_g orbitals to VBM and CBM, and thus, $LiMn_2O_4$ has similar E_g with $ZnMn_2O_4$. Compared with $ZnFe_2O_4$, the extra electron on the e_g orbital of Fe^{4+} raises the VBM to the Fermi level and makes $LiFe_2O_4$ a metal. Analogously, the single e_g electron of Ni^{3+} makes $ZnNi_2O_4$ a half-metal, while $LiNi_2O_4$ is a semiconductor because Ni^{4+} is a Jahn–Teller inactive ion with fully occupied t_{2g} orbitals but empty e_g orbitals. To evaluate the quality of the above-mentioned quantum chemical calculations, we compared the present results with

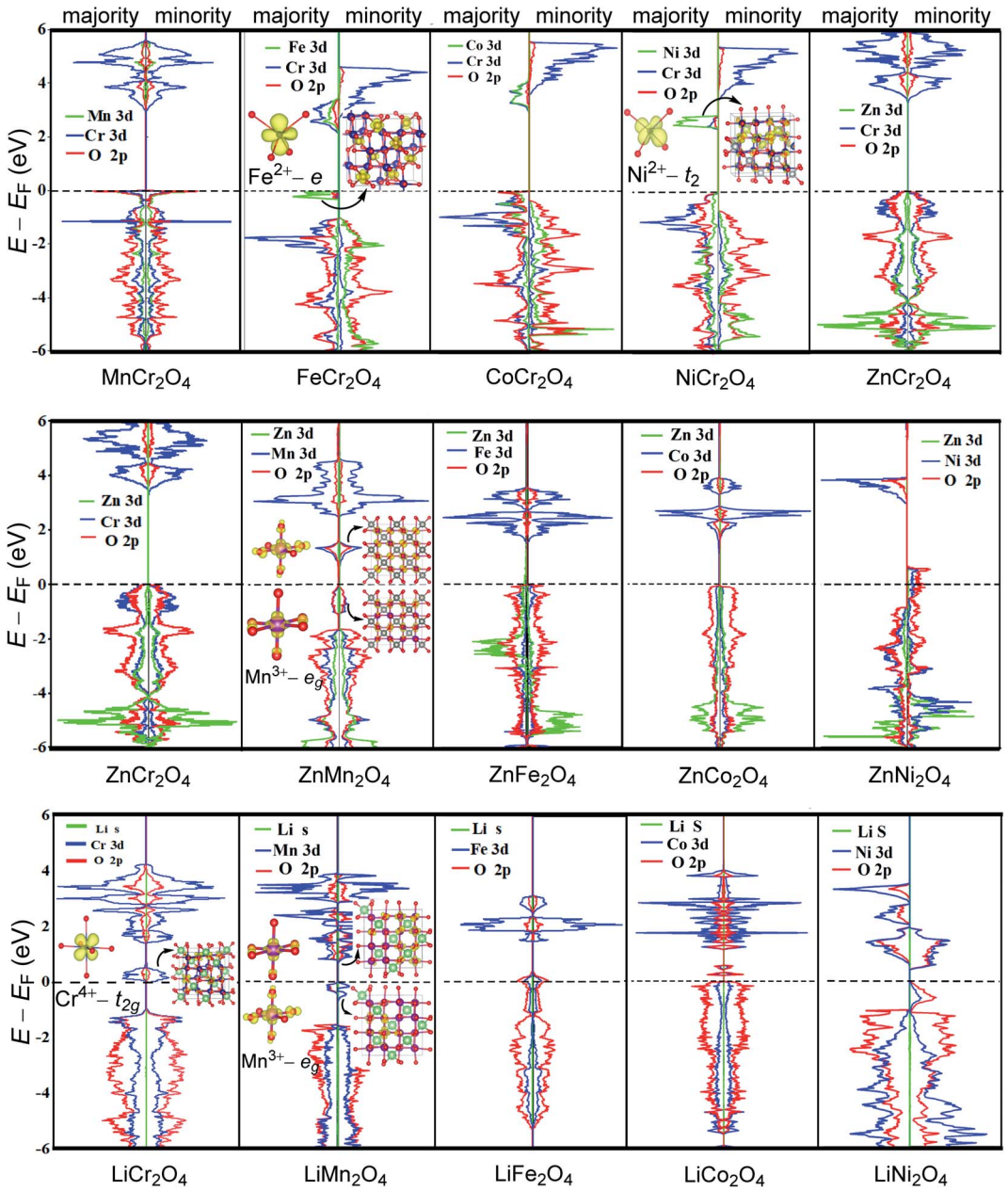

Fig. 4 The spin-resolved PDOS of ACr_2O_4 (A = Mn, Fe, Co, Ni, and Zn) and Zn/LiB_2O_4 (B = Cr, Mn, Fe, Co and Ni). The partial charge density populations corresponding to some specific states are also illustrated.

experimental data and listed the theoretically calculated and experimentally measured band gaps in Table 1. The scatter of the band gap values is associated with different determining methods. Most of the Exp. E_g values listed in Table 1 are optical band gaps obtained by UV-Vis absorption[49,51,54–56,58,59,64] or diffuse reflectance spectroscopy.[46,52] The values indicate that the calculated band gaps of $FeCr_2O_4$, $CoCr_2O_4$, $ZnCr_2O_4$, $ZnFe_2O_4$, $ZnCo_2O_4$ and $LiMn_2O_4$ accord well with the experimental measured values with errors within 0.5 eV.

In summary, the configuration of cation B has notable influence on the electronic structure of spinels. The Jahn–Teller active ions Fe^{2+}, Ni^{2+}, Mn^{3+}, Ni^{3+}, Cr^{4+} and Fe^{4+} can remarkably regulate the E_g of spinels and even change the electroconductibility.

Conclusions

The spinels are promising low-cost catalysts. Unravelling the structure–performance relationship is the foundation to realize the rational design of spinel-based catalysts. Herein, the effects of cations in tetrahedral and octahedral sites on the electronic structures of spinels were systematically investigated *via* GGA + U calculations. Three series of spinels with varying A and B, namely ACr_2O_4 (A = Mn, Fe, Co, Ni, and Zn) and Zn/LiB_2O_4 (B = Cr, Mn, Fe, Co and Ni), were elected as the model system. The results indicate that the magnetism of spinels depends on the indirect exchanges of cations (J_{MM}). The configurations of B cations in an octahedral O environment, rather than the A in

tetrahedral ones have notable influence on the electronic structures of spinels. The Jahn–Teller active ions Fe^{2+}, Ni^{2+}, Mn^{3+}, Ni^{3+}, Cr^{4+} and Fe^{4+} can remarkably regulate the band gaps of spinels and even change their electroconductibilities. The results will provide theoretical insights into the electronic properties of 3d transition metal spinels.

Author contributions

Chunyu Li: data curation, investigation, writing – original draft. Peng Li: investigation. Leyun Li: investigation. Dingjia Wang: investigation. Xingfa Gao: supervision. Xuejiao J. Gao: project administration, writing – review & editing.

Conflicts of interest

There are no conflicts to declare.

Acknowledgements

This work was supported by the National Natural Science Foundation of China (NSFC) Project (21907043 and 21773095), the Natural Science Foundation of Jiangxi, China (20202BABL213013).

Notes and references

1 W. H. Bragg, *Philos. Mag.*, 1915, **30**, 305–315.
2 M. G. Brik, A. Suchocki and A. Kamińska, *Inorg. Chem.*, 2014, **53**, 5088–5099.
3 Q. Zhao, Z. Yan, C. Chen and J. Chen, *Chem. Rev.*, 2017, **117**, 10121–10211.
4 N. R. D. Fino, G. Saracco and V. Specchia, *J. Catal.*, 2006, **242**, 38–47.
5 Q. Chen, Z. Tang, H. Lia, Q. Zhao and B. Pana, *Chem. Eng. J.*, 2020, **381**, 122656.
6 G. S. H. Michael Woodhouse and B. A. Parkinson, *Chem. Mater.*, 2005, **17**, 4318–4324.
7 D. Bhattacharya, A. Baksi, I. Banerjee, R. Ananthakrishnan, T. K. Maiti and P. Pramanik, *Talanta*, 2011, **86**, 337–348.
8 N. Dhandapani, A. Rebekah, C. Viswanathan and P. Nagamony, *Mater. Res. Bull.*, 2017, **95**, 1–8.
9 V. Figueroa-Espí, A. Alvarez-Paneque, M. Torrens, A. J. Otero-González and E. Reguera, *Colloids Surf., A*, 2011, **387**, 118–124.
10 C. M. Hussain and B. Kharisov, *Advanced Environmental Analysis. Applications of Nanomaterials*, 2016.
11 S. Mumtaz, L.-S. Wang, M. Abdullah, S. Z. Hussain, Z. Iqbal, V. M. Rotello and I. Hussain, *J. Phys. D: Appl. Phys.*, 2017, **50**, 11LT02.
12 X. Niu, Y. Xu, Y. Dong, L. Qi, S. Qi, H. Chen and X. Chen, *J. Alloy. Compd.*, 2014, **587**, 74–81.
13 Y. Peng, Z. Wang, W. Liu, H. Zhang, W. Zuo, H. Tang, F. Chen and B. Wang, *Dalton Trans.*, 2015, **44**, 12871–12877.
14 R. Sahoo, S. Santra, C. Ray, A. Pal, Y. Negishi, S. K. Ray and T. Pal, *New J. Chem.*, 2016, **40**, 1861–1871.
15 W. Shi, X. Zhang, S. He and Y. Huang, *Chem. Commun.*, 2011, **47**, 10785–10787.
16 L. Su, W. Qin, H. Zhang, Z. U. Rahman, C. Ren, S. Ma and X. Chen, *Biosens. Bioelectron.*, 2015, **63**, 384–391.
17 A. A. Vernekar, T. Das, S. Ghosh and G. Mugesh, *Chem.–Asian J.*, 2016, **11**, 72–76.
18 Z. Yang, F. Ma, Y. Zhu, S. Chen, C. Wang and X. Lu, *Dalton Trans.*, 2017, **46**, 11171–11179.
19 K. Zhang, W. Zuo, Z. Wang, J. Liu, T. Li, B. Wang and Z. Yang, *RSC Adv.*, 2015, **5**, 10632–10640.
20 C. Wei, Z. Feng, G. G. Scherer, J. Barber, Y. Shao-Horn and Z. J. Xu, *Adv. Mater.*, 2017, **29**, 1606800.
21 S. H. Lee, C. Broholm, T. H. Kim, W. Ratcliff and S. W. Cheong, *Phys. Rev. Lett.*, 2000, **84**, 3718–3721.
22 A. B. Sushkov, O. Tchernyshyov, W. R. Ii, S. W. Cheong and H. D. Drew, *Phys. Rev. Lett.*, 2005, **94**, 137202.
23 V. Kocsis, S. Bordács, D. Varjas, K. Penc, A. Abouelsayed, C. A. Kuntscher, K. Ohgushi, Y. Tokura and I. Kézsmárki, *Phys. Rev. B: Condens. Matter Mater. Phys.*, 2013, **87**, 064416.
24 F. Zhou, M. Cococcioni, C. A. Marianetti, D. Morgan and G. Ceder, *Phys. Rev. B: Condens. Matter Mater. Phys.*, 2004, **70**, 235121.
25 F. Zasada, J. Grybos, P. Indyka, W. Piskorz, J. Kaczmarczyk and Z. Sojka, *J. Phys. Chem. C*, 2014, **118**, 19085–19097.
26 V. B. O. Peña, T. Guizouarn, E. Meza and J. L. Gautier, *Bol. Soc. Esp.*, 2004, **43**, 736–739.
27 M. R. Suchomel, D. P. Shoemaker, L. Ribaud, M. C. Kemei and R. Seshadri, *Phys. Rev. B: Condens. Matter Mater. Phys.*, 2012, **86**, 054406.
28 G. Kresse, *Phys. Rev. B: Condens. Matter Mater. Phys.*, 1996, **54**, 11169–11186.
29 P. E. Blöchl, *Phys. Rev. B: Condens. Matter Mater. Phys.*, 1994, **50**, 17953–17979.
30 J. P. Perdew, K. Burke and M. Ernzerhof, *Phys. Rev. Lett.*, 1996, **77**, 3865–3968.
31 H. J. Monkhorst and J. D. Pack, *Phys. Rev. B: Solid State*, 1976, **13**, 5188–5192.
32 V. V. Anisimov, J. Zaanen and O. K. Andersen, *Phys. Rev. B: Condens. Matter Mater. Phys.*, 1991, **44**, 943–954.
33 S. L. Dudarev, G. A. Botton, S. Y. Savrasov, C. J. Humphreys and A. P. Sutton, *Phys. Rev. B: Condens. Matter Mater. Phys.*, 1998, **57**, 1505–1509.
34 D. Debashish and S. Ghosh, *J. Phys. D: Appl. Phys.*, 2015, **48**, 425001.
35 D. Andersson and C. Stanek, *Phys. Chem. Chem. Phys.*, 2013, **15**, 15550–15564.
36 D. Santos-Carballal, A. Roldan, R. Grau-Crespo and N. H. de Leeuw, *Phys. Rev. B: Condens. Matter Mater. Phys.*, 2015, **91**, 195106.
37 J. S. Zhou and J. B. Goodenough, *Phys. Rev. Lett.*, 2006, **96**, 247202.
38 K. Ueda, H. Tabata and T. Kawai, *Science*, 1998, **280**, 1064.
39 J. Kanamori, *J. Appl. Phys.*, 1960, **31**, S14–S23.
40 J. Kanamori, *J. Phys. Chem. Solids*, 1959, **10**, 87–98.
41 J. Kanamori, *Prog. Theor. Phys.*, 1957, **17**, 177–196.

42 J. B. Goodenough and J. S. Zhou, in *Localized to Itinerant Electronic Transition in Perovskite Oxides*, Springer Berlin Heidelberg, Berlin, Heidelberg, 2001.
43 J. B. Goodenough, *J. Phys. Chem. Solids*, 1958, **6**, 287–297.
44 J. B. Goodenough, *Phys. Rev.*, 1955, **100**, 564–573.
45 N. Mufti, A. A. Nugroho, G. R. Blake and T. T. M. Palstra, *J. Phys.: Condens. Matter*, 2010, **22**, 075902.
46 V. Kocsis, S. Bordács, D. Varjas, K. Penc, A. Abouelsayed, C. A. Kuntscher, K. Ohgushi, Y. Tokura and I. Kézsmárki, *Phys. Rev. B: Condens. Matter Mater. Phys.*, 2013, **87**, 064416.
47 C. Benhalima, S. Amari, L. Beldi and B. Bouhafs, *Spin*, 2019, **09**, 1950014.
48 D. E. C. G. Shirane and S. J. Pickart, *J. Appl. Phys.*, 1964, **35**, 954.
49 T. L. S. L. Wijesighe and D. J. Blackwood, *J. Phys.: Conf. Ser.*, 2006, **28**, 74–78.
50 M. Akyol, İ. Adanur, A. O. Ayaş and A. Ekicibil, *Phys. B*, 2017, **525**, 144–148.
51 I. Efthimiopoulos, Z. T. Y. Liu, S. V. Khare, P. Sarin, T. Lochbiler, V. Tsurkan, A. Loidl, D. Popov and Y. Wang, *Phys. Rev. B: Condens. Matter Mater. Phys.*, 2015, **92**, 064108.
52 M. Enhessari, A. Salehabadi, S. Khanahmadzadeh, K. Arkat and J. Nouri, *High Temp. Mater. Processes*, 2017, **36**, 121–125.
53 H. J. Kim, I. C. Song, J. H. Sim, H. Kim, D. Kim, Y. E. Ihm and W. K. Choo, *Solid State Commun.*, 2004, **129**, 627–630.
54 Y. Benrighi, N. Nasrallah, T. Chaabane, V. Sivasankar, A. Darchen and O. Baaloudj, *Opt. Mater.*, 2021, **115**, 111035.
55 Q. Wang, J. Chen, H. Lu, P. Huang, J. Wang, M. Li, Y. Lu, G. Chang, Z. C. Feng and Y. He, *Appl. Surf. Sci.*, 2019, **475**, 820–827.
56 R. Gherbi, Y. Bessekhouad and M. Trari, *J. Phys. Chem. Solids*, 2016, **89**, 69–77.
57 W. P. W. Schiessl, H. Karzel, M. Steiner and G. M. Kalvius, *Phys. Rev. B: Condens. Matter Mater. Phys.*, 1996, **53**, 9143–9152.
58 N. Kislov, S. S. Srinivasan, Y. Emirov and E. K. Stefanakos, *Mater. Sci. Eng., B*, 2008, **153**, 70–77.
59 H. Guo, J. Chen, W. Weng, Q. Wang and S. Li, *Chem. Eng. J.*, 2014, **239**, 192–199.
60 M. Lauer, R. Valenti, H. Kandpal and R. Seshadri, *Phys. Rev. B: Condens. Matter Mater. Phys.*, 2004, **69**, 75117.
61 C. Y. Ouyanga, S. Q. Shib and M. S. Leid, *J. Alloys Compd.*, 2009, **474**, 370–374.
62 D. Santos-Carballal, P. Ngoepe and N. Leeuw, *Phys. Rev. B*, 2018, **97**, 085126.
63 G. R. J. Rodríguez-Carvajal, Masquelier and M. Hervieu, *Phys. Rev. Lett.*, 1998, **81**, 4660–4663.
64 V. Paulraj, B. Swami and K. Kamala Bharathi, *Appl. Phys. Lett.*, 2019, **115**, 093901.
65 Y. Mouhib, M. Belaiche, C. A. Ferdi, M. Lacham and A. Elacham, *New J. Chem.*, 2020, **44**, 2538–2546.
66 M. G. S. R. Thomas, W. I. F. David and J. B. Goodenough, *Mater. Res. Bull.*, 1985, **93**, 473–476.
67 O. Tchernyshyov, R. Moessner and S. L. Sondhi, *Phys. Rev. Lett.*, 2002, **88**, 067203.
68 Y. Yamashita and K. Ueda, *Phys. Rev. Lett.*, 2000, **85**, 4960–4963.